EPRG-PRCI-APGA
23rd Joint Technical Meeting
Edinburgh, Scotland
6–10 June 2022

EPRG-PRCI-APGA
23rd Joint Technical Meeting
Edinburgh, Scotland • 6–10 June 2022

PAPER TITLE: CORROSION UNDER DISBONDED COATINGS: WHY, WHEN AND HOW IT OCCURS ON BURIED PIPELINES

PAPER NUMBER: 6

Mike YJ Tan
Deakin University, School of Engineering, Victoria, Australia

Facundo Bob Varela*
Deakin University, School of Engineering, Victoria, Australia

Ying Huo
Deakin University, School of Engineering, Victoria, Australia

* presenting author

ABSTRACT

Corrosion under disbonded coatings (CUDC) occurs frequently on the external surfaces of buried and submerged steel structures such as underground pipelines. CUDC causes many types of corrosion damage such as crevice corrosion, pitting, microbiologically induced corrosion and stress corrosion cracking. According to industry advisers, approximately 90% of corrosion occurring on buried gas pipelines was due to corrosion under disbonded coatings and heat shrink sleeves (behaving like a shielding coating). The industry concerns are that this type of corrosion cannot be mitigated by conventional cathodic protection (CP) due to shielding by disbonded coatings/ heat shrink sleeve/concrete casings or cannot be detected through normal inspection and survey means. The inability to mitigate and detect the corrosion leads to accelerated localized corrosion under disbonded coatings going unnoticed., Therefore, aged pipelines with disbonded shielding coatings have been identified as prime 'high risk' pipelines.

Laboratory experimental findings on CUDC using innovative electrode array corrosion probes have been reported. Recently electrode array corrosion probes have been installed at six pipeline sites around Victoria, Australia aimed at visualizing and probing localized corrosion of buried steel pipelines under simulated disbonded coatings and heat shrink sleeves. Corrosion data have been successfully received on-site and remotely, providing first-hand information on why, when and how CUDC occurs on buried pipelines.

This article summarizes new findings from recent big sand box and fielding tests. Sand box and field tests have repeatedly confirmed that corrosion under disbonded coatings or wraps is significantly affected by soil environmental conditions and changes in those conditions. Major CUDC events were found to occur when there was a dry-wet change in soil. This finding suggests that active CUDC occurs to a CP-protected pipeline only over certain periods (e.g. dry-wet seasonal change periods). Over these periods of CUDC activity normal CP levels are insufficient to mitigate the high corrosion rates. It was also confirmed that coating disbondment geometry, pH and soil saturation status are key parameters affecting CUDC. The discussion is extended to potential methods for controlling CUDC, and methods for early detection, diagnosis, modelling, and prediction of localized corrosion of buried pipelines.

DISCLAIMER

1. INTRODUCTION

Buried and submerged metallic structures such as underground steel pipelines are usually protected against corrosion by organic coatings in conjunction with CP. Organic coatings protect metallic substrates primarily by acting as a barrier for corrosive species such as water, ions and oxygen. Unfortunately, coatings usually contain various forms of defects such as pores, and can crack or degrade under mechanical impacts and environmental effects, resulting in the formation of pathways for corrosive species to reach the metal substrate. Under excessive CP, coatings can disbond, causing the corrosion mechanism to change from the initial general soil corrosion to much more complex localized corrosion usually referred to as corrosion under disbonded coatings (CUDC), as illustrated in Figure 1.

Coating disbondment and CUDC are considered to be the worst-case scenario form of materials degradation and corrosion that occur frequently on the external surface of buried steel structures such as underground pipelines. CUDC has been extensively studied with many reports in the literature including those in references [1-4]. It is generally accepted that coating disbondment forms a crevice between the metal surface and the disbonded coating layer that provides easy lateral paths for corrosive species to reach the metal surface while simultaneously shielding cathodic protection currents from reaching the metal substrate. Although cathodic shielding is well-known to be a major factor contributing to CUDC, there is insufficient understanding of other factors affecting the initiation, propagation or termination of CUDC probably due to the lack of visibility of CUDC on buried pipes.

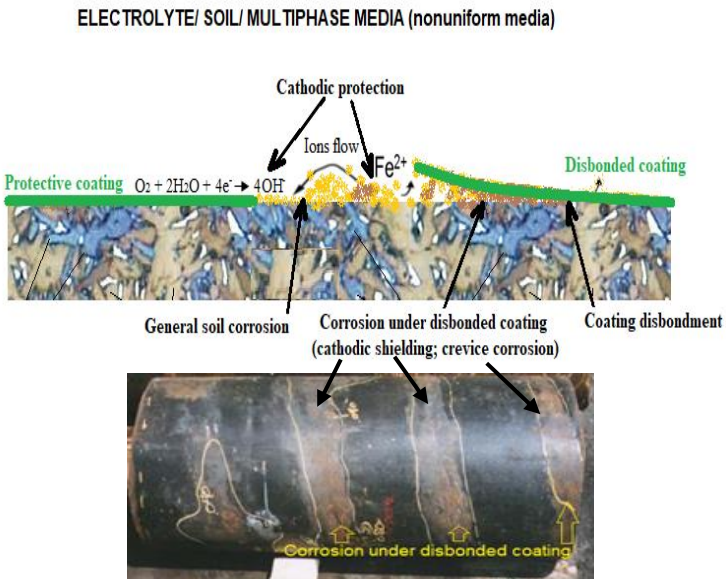

Figure 1. Illustrating CUDC over a steel surface with damaged and disbonded coating.

Over the past decade, the authors have conducted extensive research to understand and quantify the cathodic disbondment behaviour of pipeline coatings [5-8], the cathodic shielding behaviour of disbonded coating films [9,10], as well as localised corrosion under disbonded coatings in electrolyte solution [11-13] and in soil [14,15]. Taking advantage of the high temporal and spatial resolution of an electrochemically integrated multi-electrode array, coating disbondment and CUDC have been

visualized [5-8,11-15], facilitating its study. The electrode array method was used for probing localised electrode processes evolving and propagating dynamically on pipeline steel surfaces under the effect of cathodic shielding and coating disbondment [11-15]. Various laboratory devices and probes have been designed to simulate a disbonded coating using intact coating membranes in order to assess the penetration and contribution of CP currents through coating films. Disbondment geometry, pH and soil saturation status have been shown to be key parameters affecting CUDC. For instance, it was found that in non-saturated soil CUDC behaviour changed significantly with coating disbondment gap size [14,15]. The effect of CP current shielding by disbonded coating film on CUDC has also been assessed using a method developed for precisely measuring CP current penetration [9,10]. The main results indicate that the majority of the tested coatings, with thicknesses typically used in the field, will shield CP in the intact condition [9,10].

Recently we have conducted further tests in the pipeline field and in big sandboxes in order to further understand and quantify the impact of various factors on coating disbondment and CUDC, with particular focus on soil wet-dry changes and CP interruptions [16,17]. This paper provides an overview of major findings regarding factors affecting the initiation, propagation and termination of CUDC on buried steel.

2. TESTING METHODS

Over the past decade, corrosion probes designed based on electrochemically integrated multi-electrode arrays have been used in the laboratory [5-8,11-15] and also in the field and semi-field sandboxes to visualize, probe and monitor critical forms of buried steel corrosion [1]. Probes for simulating and measuring CUDC were made and deployed at underground pipeline sites and laboratory sandboxes. Figure 2(a)-(c) show the electrode array probes designed for monitoring of CUDC. The probes used in this work consisted of 100 closely packed, but isolated square shaped pipeline steel X65 electrodes (e.g. 2.44 mm× 2.44 mm) embedded in epoxy resin. The gaps between neighboring electrodes were kept small (e.g. 0.10 ± 0.05 mm). After grinding using a SiC 600 grit paper, the probe was installed in specifically designed field sites or a sandy soil box testing cells, as illustrated in Figures 3 and 4. These probes are made to create the conditions produced under disbonded coatings, incorporating a polymethyl methacrylate (PMMA) cover that behaves as a perfectly shielding coating (Figure 2(b)) or an epoxy pipeline coating film (Figure 2(c)). This cover or film was placed at a constant distance of 1 mm from the electrodes surface to create a crevice that was considered to create the 'worst case scenario' CUDC condition [14,15]. In order to maximise the length of the crevice, the electrode array consisted of 4 row of 25 square electrodes. The first two columns of electrodes directly were left to be exposed to the corrosive environment, simulating the coating holiday usually found next to disbonded areas. More details on the CUD probe tests in the laboratory have been included references [14,15].

Field tests were conducted by deploying CUD probes in four gas pipeline sites in Melbourne and Geelong regions Australia. Table 1 presents details about each installation site environmental conditions where steel pipelines covered with different coating materials existed. Please note that the soil resistivity varied from site to site and from season to season. Table 2 shows details of the probes' CP and open circuit potentials recordings. Figure 3 illustrates probes field installation and basic electrical connection at each installation site. Figure 4 illustrates accelerated semi-field tests performed in sandboxes of one meter in size with an epoxy coating coated pipe, 220 mm in diameter installed across. As shown in the figure, the arrangement consisted of titanium strips 2.5 cm wide installed at the four vertical edges of the box as anodes for the CP system. A copper / copper sulphate reference electrode was installed next to the centre of the front wall of the sandbox. The corrosion probe was installed at approximately the same depth as the centre line of the simulated pipeline at a distance of 20cm from it. At the beginning of the test, once all probes were installed and the box was filled with pre-washed sand up to a total depth of 60 cm. Tap water was added to the box until a 10 cm supernatant solution was stable above the sand to maintain a saturated environment for 24 h. After the drainage valve was open, the system was left to evolve for approximately 2 weeks before the wet/dry cycles were reinitiated by closing the drainage valve and adding tap water once again. This simulates the dry/wet cycles in industry pipeline

field that are due to weather/rainfall changes, commonly forming air gaps under disbonded coatings. At all times the simulated pipeline section and the probes were kept at a CP potential of -850 mV_{CSE}.

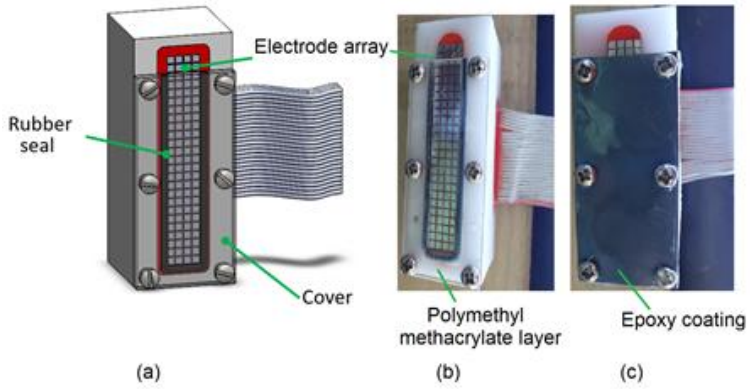

Figure 2. Ilustration of (a) the CUDC probes desings for simulating corrosion under disbonded coating by partially covering most of the electrode array with (b) an acrylic or (c) an epoxy pipeline coating layer that behaves as a shielding coating.

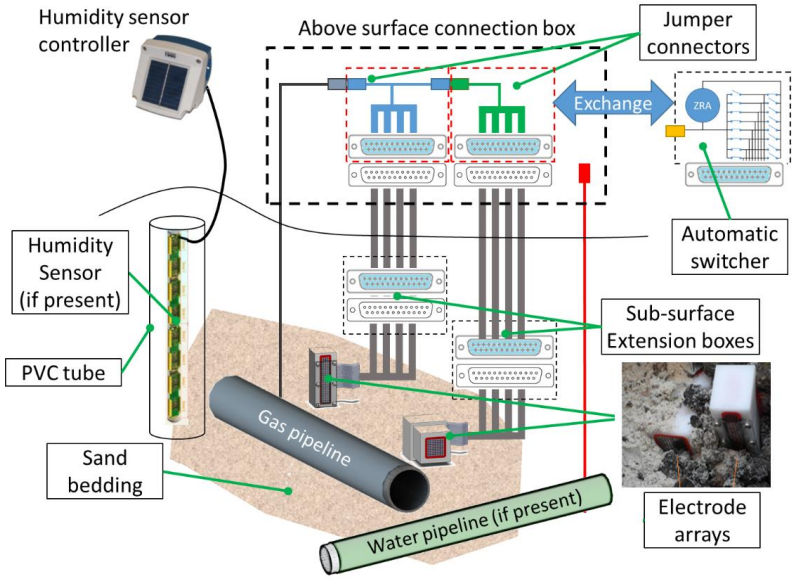

Figure 3. Schematic representation of a probe installation site and basic electrical connection performed at each installation site.

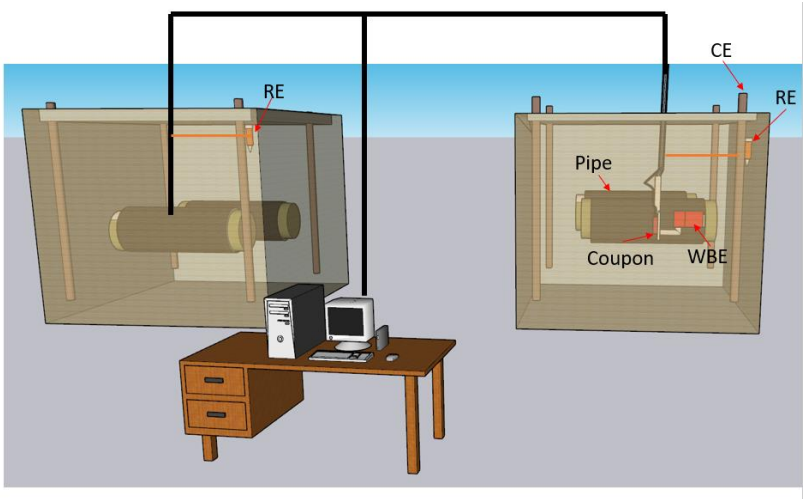

Figure 4. Sandbox test setups for CUDC testing.

Table 1 Details of the probe's installation site conditions [17].

Tag	Site	Pipelines present	Bedding material	Observations during the installation
A	North of Melbourne	Cross-bonded water and gas pipelines	Sand	The pipe was located beneath a concrete slab.
B	West of Melbourne	Cross-bonded water and gas pipelines	Sand	Independent connection to both pipelines.
C	North of Melbourne	Gas Pipeline	Sand	Underground running water present.
D	Geelong	Gas Pipeline	Sand	Clay rich soil.

Table 2. Probe field installation site CP and open circuit potentials recordings [17].

Tag	Connected to	Potential vs. Cu/CuSO4 reference electrode	
		Min	Max
A	Gas pipeline	-1020mV	-980mV
	Open circuit	-877mV	-680mV
B	Gas pipeline	-1050mV	-916mV
	Water and Gas Pipelines	-791mV	-769mV
	Water pipeline	-530mV	-501mV
	Open circuit	-780mV	-752mV
C	Gas pipeline	-1850mV	-1380mV
	Open circuit	-1060mV	-980mV
D	Gas pipeline	-1426mV	-1320mV
	Open circuit	-920mV	-830mV

Measurements were performed regularly to provide in-situ and site-specific view of corrosion processes affecting buried steel pipelines. Localized corrosion rates were measured with a sensitivity in the order of 10µm/year [17].

3. TEST RESULTS AND DISCUSSION

Cumulative metal loss maps for the electrode array coating disbondment probe installed in site A are presented in Figure 5 where the black vertical line represents the division between the holiday and the disbonded coating area. It can be seen in Figure 5 only minor corrosion looses occurred under the coating disbondment (the maximum metal losses were less than 30µm). Metal losses on the probe connected to gas pipeline show CP did not reduce metal losses, suggesting CP was ineffective due to CP shielding by the disbonded coating layer. The fact that similar metal losses were recorded within the crevice areas of corrosion probes with and without CP (see Figure 5) can be explained by analyzing the current distribution maps. Figure 6 presents characteristic current distribution maps obtained from probes under both gas pipeline CP and water pipeline open circuit conditions. The current distribution map obtained 4 hours after the probe's installation under gas pipeline CP shows large cathodic currents outside the crevice, while an area with cathodic and anodic currents was found over a region close to the crevice opening. Interestingly, the summation of the current densities found in this region was zero, indicating that this corrosion cell was isolated from CP outside the crevice. This type of current distribution has been found in previous studies performed using the same type of probes in non-saturated soils and it is attributed to the formation of air gaps within the coating disbondment [11,13].

Figure 7 illustrates this concept. Here the non-saturated soil surrounding the probe draws part of the solution initially placed within the crevice leaving an air gap. This air gap influences the corrosion process in two ways. One, it act as a disruption in the electrolytic path required to supply CP to the further end

of the crevice, and two, it also acts as a renewable source of oxygen for the isolated corrosion cell formed within the crevice. Depending on the passive state of the metal and on how long the solution within the crevice can remain, this condition can lead to severe localized corrosion. In the particular case of the probe installed in site A, the crevice seems to dry up by the second day of exposure when only a small corrosion cell was found at the crevice tip. After this period no significant currents were detected inside the crevice, independent of the CP condition. This suggests that for site A the wet and dry cycles that trigger this corrosion mechanism are infrequent.

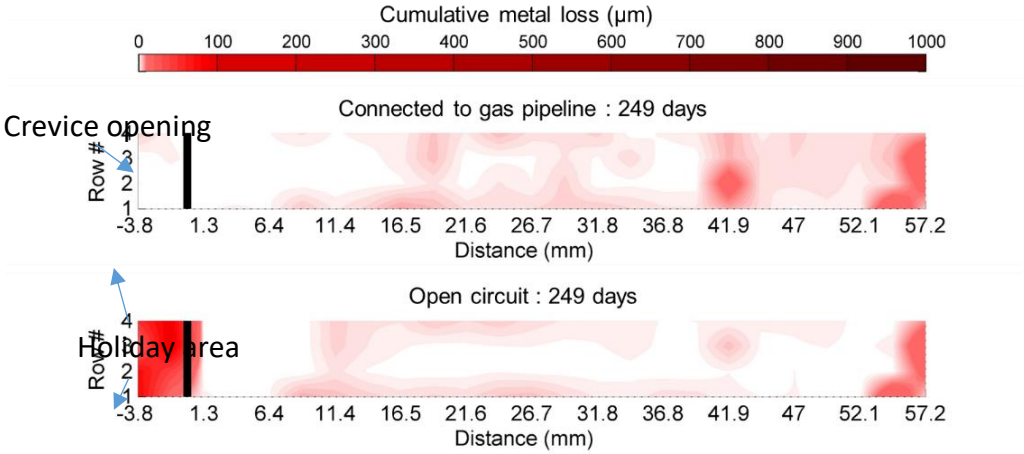

Figure 5. Final cumulative corrosion maps for the disbonded coating probe installed at site A [17].

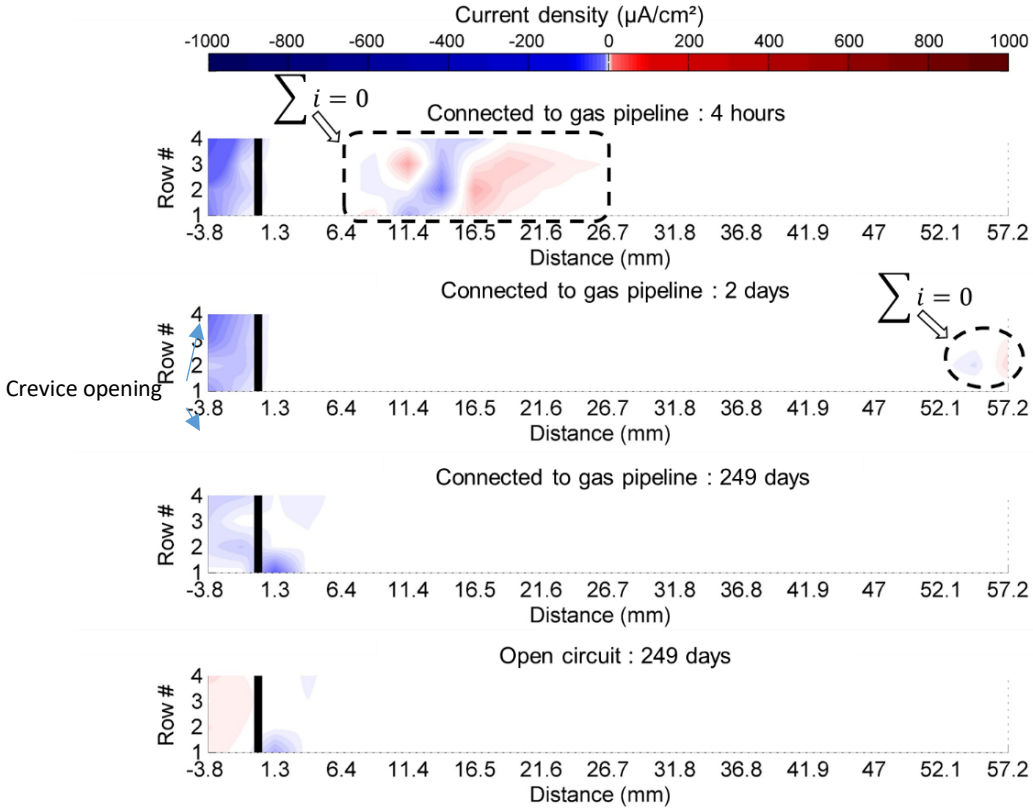

Figure 6. Evolution of the current density distribution maps on the disbonded coating probe installed at site A.

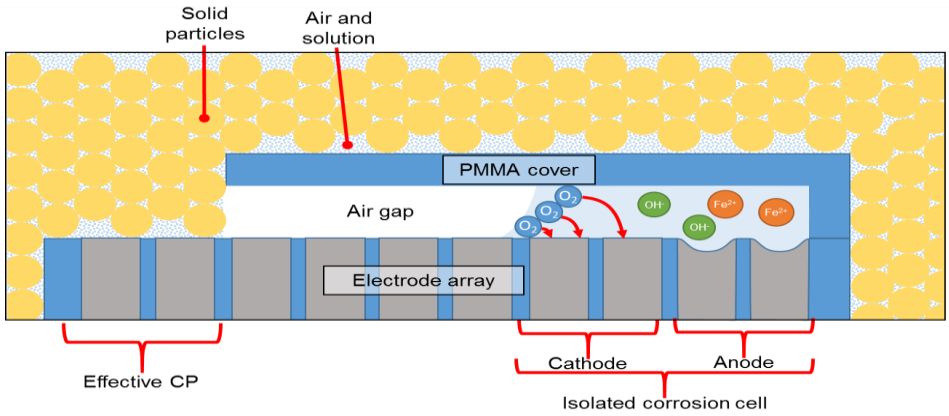

Figure 7. Schematic representation of air gap corrosion model under disbanded coating.

Figure 8 shows representative current density maps obtained from CUD probes located at the pipeline site B (a Melbourne water and gas pipelines crossing site). At the site, as detailed in Table 1, the CP potential of the gas pipeline was fluctuating between -916mV and -1050mV and the potential of the water pipeline was fluctuating between -530mV and -510mV. A major feature in current density maps shown in Figure 8 is that at the gas pipeline CP potential, as shown in Figure 8(a), the coating disbondment area was well protected with only a few anodic densities registered, while the coating disbondment area at water pipeline potential was under insufficient CP with large anodic areas clearly visible in Figure 8(b). Figures 8(c) and (d) show accumulated corrosion on the CUD probes, which indicates little corrosion on the probe under the gas pipeline CP potential but significant corrosion on the probe under water pipeline potential. This is in good agreement with the corroded surface image after the probe was withdrawn from the installation site after 661 days of testing, as shown in Figure 8(e) and the water pipeline corrosion condition shown in Figure 8(f).

In this case, the metal losses did change as a function of the CP condition and CP was working well for the gas pipeline at the site but not for the water pipeline. These results illustrate CP potential is a critical factor affecting corrosion of buried pipelines exposed to unsaturated soil. Figure 8(g) and (h) show more results from different corrosion probes during and after completing 661 days of testing. As shown in Figure 8(g), corrosion maps from the bare probe are in generally good agreement with the pitting behavior observed by visual inspection of the pipeline after 661 days of testing. Figure 8(f) compares the measured corrosion losses and their distribution over a probe surface after 661 days of testing, together with photos of the corroded probe surfaces. There is a good correlation between monitored corrosion depths and profilometry measurement results. This result demonstrates the accuracy of corrosion monitoring by the probes.

Figure 9 presents the final metal losses distribution maps for the coating disbondment probe installed at site B for all four CP conditions tested by connecting the probe to the CP protected gas pipe, to both gas and water pipes, to the unprotected water pipe, and at open circuit condition. Similarly to the results from site A, when connected to the gas pipeline, the highest metal losses were less than 30µm at the crevice tip location. At this site B, however, the metal losses did change as a function of the CP condition. Metal losses within the crevice were increasingly more generalized and intense as the probe was connected to the gas and water pipelines, to the water pipeline and left at open circuit, in that order. This suggests CP was partially available at the crevice area. The results obtained from the disbonded coating probe installed in site C and D presented similar behavior to that observed from the probe in site B.

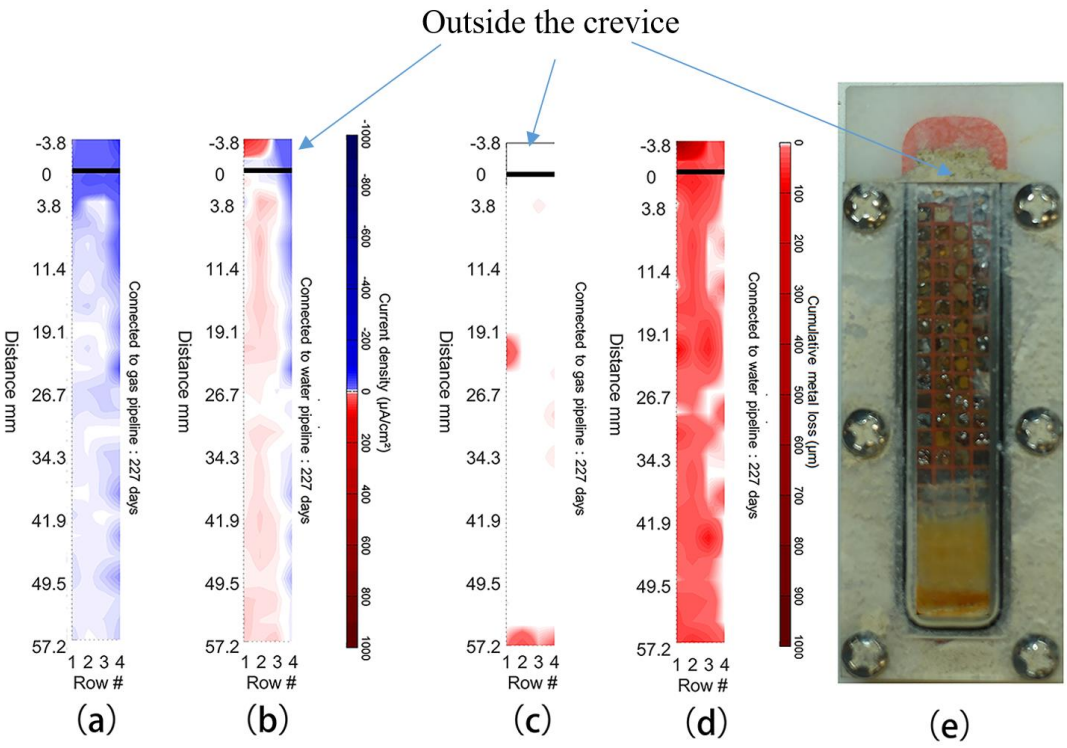
Outside the crevice
Distance mm
Row #
Connected to gas pipeline : 227 days
Connected to water pipeline : 227 days
Current density (μA/cm²)
Cumulative metal loss (μm)
(a)
(b)
(c)
(d)
(e)

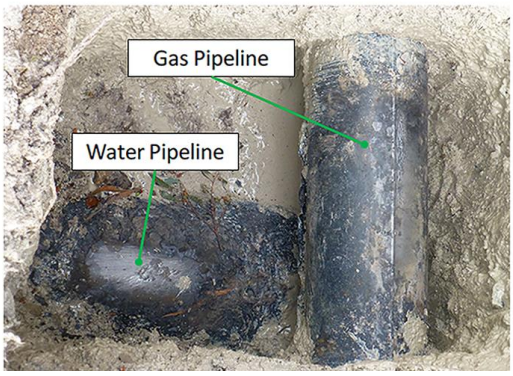
Gas Pipeline
Water Pipeline

(f)

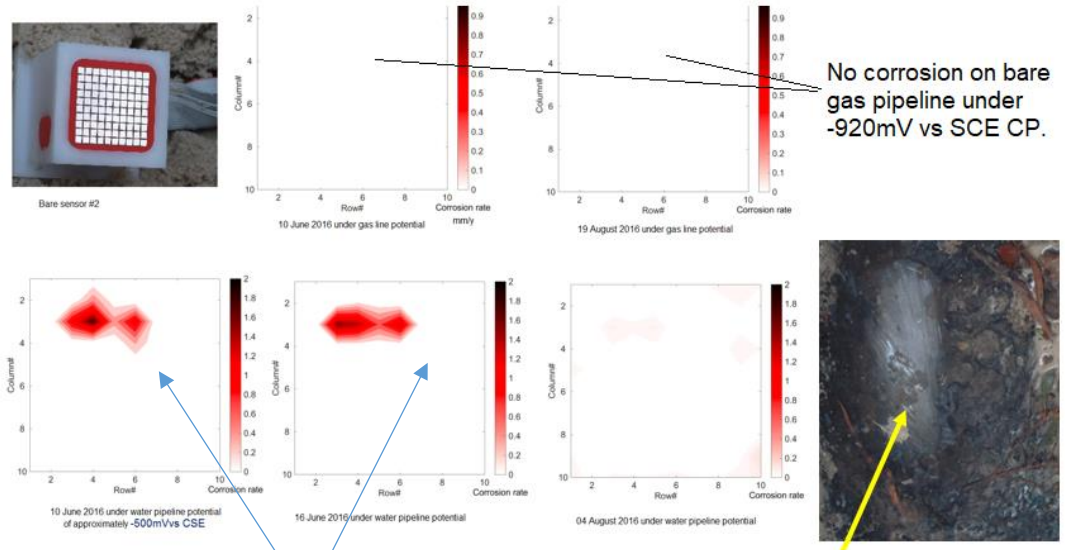
Bare sensor #2
10 June 2016 under gas line potential
19 August 2016 under gas line potential
No corrosion on bare gas pipeline under -920mV vs SCE CP.
10 June 2016 under water pipeline potential of approximately -500mVvs CSE
16 June 2016 under water pipeline potential
04 August 2016 under water pipeline potential
Pitting occurs on bare water pipeline under -500mV vs SCE CP (approximately 1mm/y at early stages). This is in agreement with observation of pits on the water pipeline surfaces.

(g)

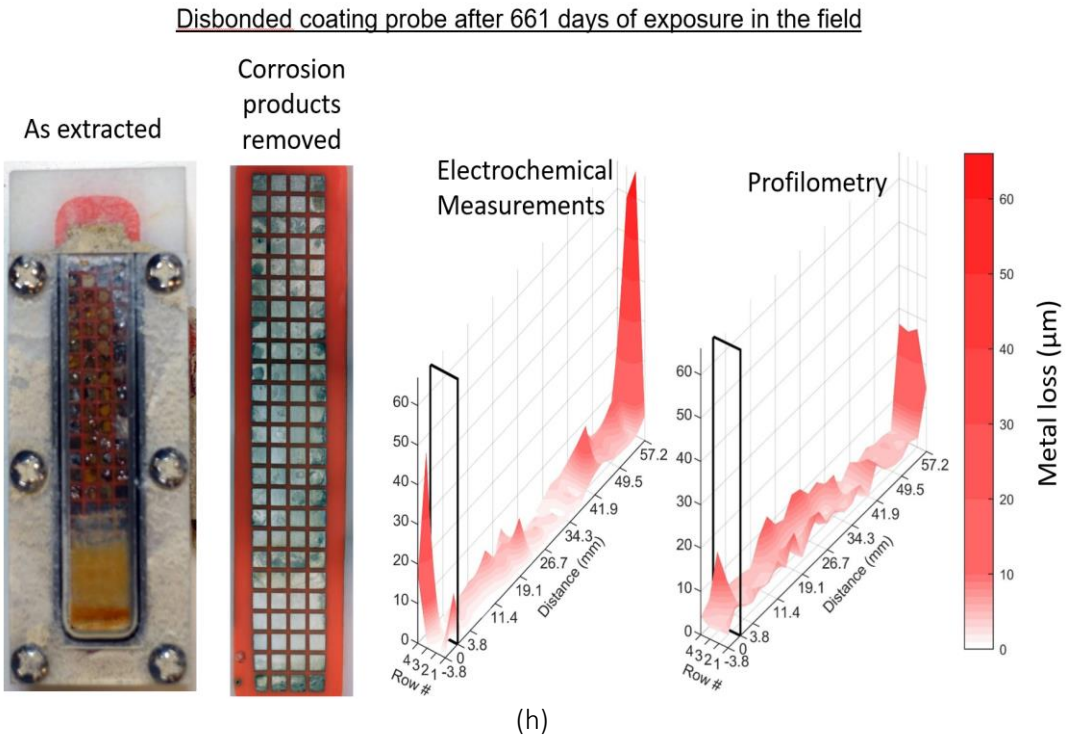

Figure 8 (a)-(b) Representative current density distribution maps over the CUDC probes installed at test site B (in the Altona North testing site, Melbourne) at gas pipeline (a) and water pipeline (b) potentials. (c)-(d) Final cumulative corrosion maps for the CUDC probes at gas (c) and water (d) pipeline potentials. (e) Image after the probe was withdrawn from the installation site after 661 days of testing. (f) Photo of the existing gas and water pipelines located at the probe installation site. (g) A summary of typical data collected from the bare steel probe simulating and monitoring bare steel corrosion at the Altona North Melbourne gas/water pipeline intersection site. (h) Illustrating the overall corrosion at site B after 661 days of field testing, from the disbonded coating probes.

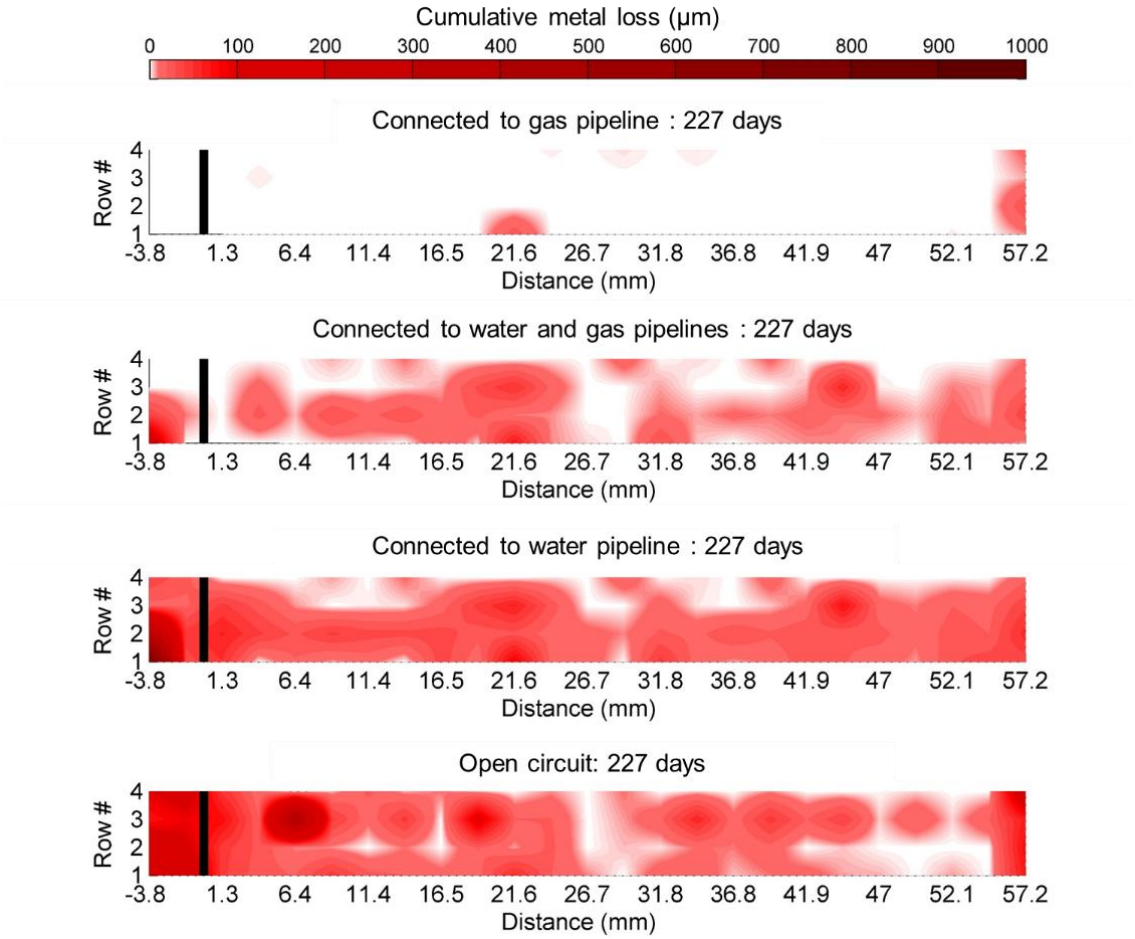

Figure 9. Final cumulative corrosion maps for the disbonded coating probe installed in site B.

A finding from the field testing using the CUDC probes is that corrosion appeared significantly affected by the wet and dry cycles of the environmental changes within the crevice. If the environment within the crevice is kept dry, no corrosion would occur. Also if the environment is wet enough to form a continuous electrolytic path, CP can be effective under the disbonded area and corrosion can be prevented. However if the environment allows the formation of isolated corrosion cells, corrosion tends to occur locally. In order to verify the relationship between corrosion susceptibility under disbonded coatings and the hydrogeological conditions around the pipe and the type of bedding soil particles, tests were conducted in sandboxes where soil conditions could be better controlled. Therefore laboratory testing in sandbox was carried out by installing CUDC probes in sandboxes that simulate wet-dry cycles, as shown in Figure 4. Figure 10 presents the current density maps obtained across the surface of the electrode array soon after the onset of the test.

The 0 days map was obtained approximately 2 hours after the addition of water to the sandbox. In this map, relatively large cathodic current densities, driven by the CP system, were found outside the crevice. Inside the crevice, a sharp decreasing gradient of cathodic current densities is found close to the crevice opening. This gradient is produced by a combination of CP shielding and by lower and lower fractions of humid sand that gets into the crevice and provides an electrolytic pathway for the CP current. For distances between 10 and 50 mm from the crevice opening, no current densities were found inside the crevice. Finally, at the very tip of the crevice a combination of anodes and cathodes was found. This current density distribution is consistent with previous finding and the model in Figure 7 that the large area of zero current density inside the crevice was related to the formation of an air gap that isolated the area where CP is effective from the solution remaining inside the crevice, allowing the formation of isolated corrosion cells. These results further suggest that the formation of 'zero current' zones should be due to the solution drying up to form 'air gaps'.

After five days, the current density distribution map changed considerably. Outside the crevice and at the crevice opening, current densities were significantly less cathodic, and even some small anodic current were measured. This is due to the lower humidity of the environment. Inside the crevice, another isolated corrosion cell was formed near the centre of the crevice area and the corrosion cell at the bottom of the crevice presumably dried off. Figure 11 presents a series of current distribution maps that illustrate the changes observed for the 2nd an 3rd wet-dry cycle. At the beginning of the cycle, when water was added to the box, the isolated corrosion cells at the crevice tip and centre of the array were reactivated. Then, the electrochemical activity on both corrosion cells decreased through the rest of the cycle. For the cell at the crevice tip the decrease was abrupt, but for the cell at the centre of the array the decrease was slow, taking up to 14 days to shut off the corrosion cell. From the fourth wet-dry cycle on, the behaviour was different (Figure 12). In these cases the addition of water at the start of the cycle did not reactivate any isolated electrochemical cells inside the crevice. Instead, only an increase of cathodic current densities was found outside the crevice and at the crevice opening where CP is effective. For the rest of the cycle only an initial decrease in cathodic current density at the same area was observed. From then on, no significant changes were registered.

Figure 13 presents the surface of the array, the profilometry results reflecting actual metal loss and the electrochemically calculated metal losses based on the probes. The surface of the sensor presented three areas with significant deposition of corrosion products. In all three cases the corrosion product mixed with sand to form a deposit that was well attached to the steel surface. It is believed that the formation of this bulky corrosion product-sand mix at the outside of the crevice gradually prevented water ingress. This could explain the differences observed between the current densities maps obtained during the first three wet-dry cycles and from the 4th cycle on (Figure 4.39). The corrosion observed outside the crevice might have been produced during the two CP interruptions. The profilometry results indicate that metal losses outside the crevice were 27 µm at the most, while at the centre and bottom of the array, maximum values were closer to 50 µm. The electrochemically calculated metal losses, show an extremely good correlation with the pattern that corrosion presented inside the crevice, and the magnitude of the maximum metal losses.

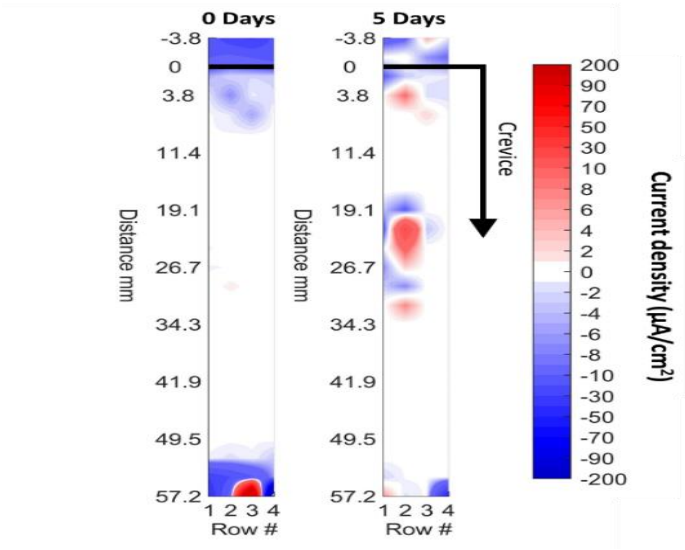

Figure 10. Current density distribution maps for the 1st wet-dry cycle.

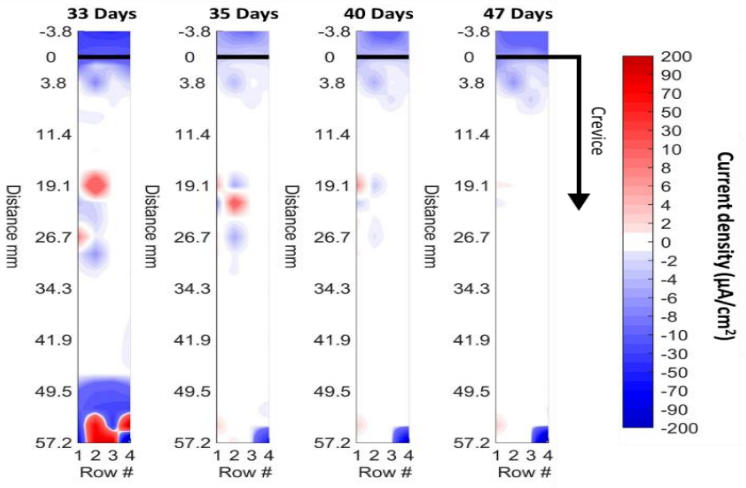

Figure 11. Current density distribution maps typical of the 2nd and 3rd wet-dry cycle.

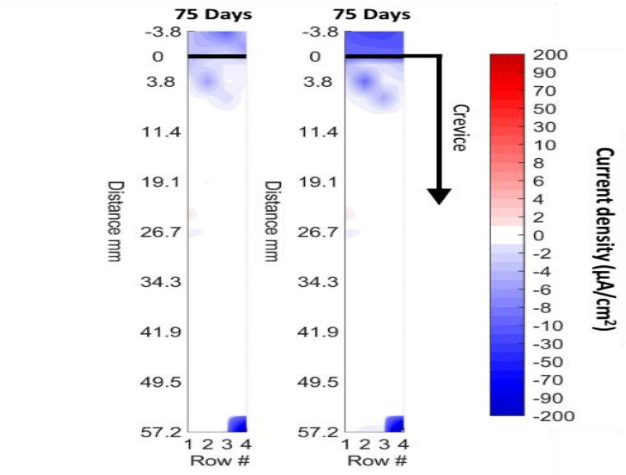

Figure 12. Typical current density distribution maps from the 4th wet-dry cycle on.

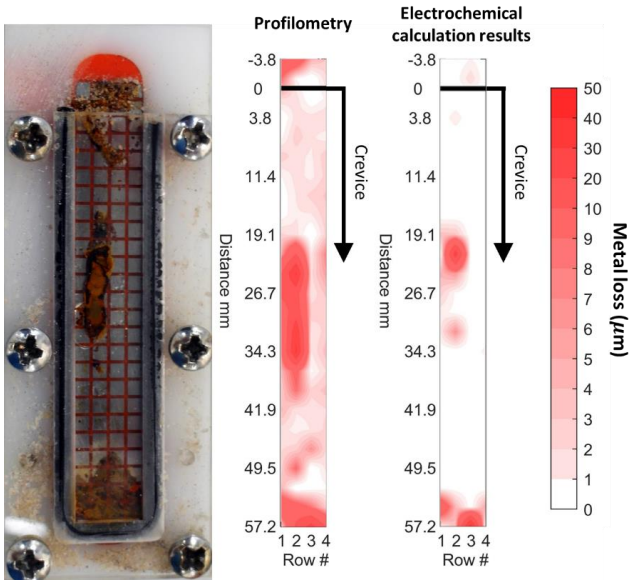

Figure 13. Appearance of the electrode after testing, profilometry results after corrosion product removal and results of electrochemically calculated metal loss.

Figure 14 shows a sample series of results from another sandbox test that simulates a corrosion probe buried in a sandy soil environment. Figure 14 depicts current density distribution maps recorded at various test periods under different CP and wet-dry conditions. In these maps, anodic/corrosion current densities are indicated by positive numbers, whereas cathodic/CP current densities are indicated by negative values. Figure 14(a) illustrates corrosion starting immediately after the sand was saturated by 0.01M/L NaSO4 solution, showing anodic dissolution and cathodic reaction currents. As shown in Figure 14(b), when CP was applied for 2 hours (at -1.5V vs. CSE) no anodic dissolution current can be seen and full cathodic protection was applied on the corrosion probe surface. As shown in Figures 14(c) and 14(d), when the electrolyte was drained from the sandbox changes to the maps occurred, showing anodic activities. This shows that corrosion occured when the sand was dried, simulating wet-dry season changes. Many anodes appear under the crevice area (simulating disbonded coating area), suggesting wet-dry cycle is a major concern for corrosion under disbondment corrosion.

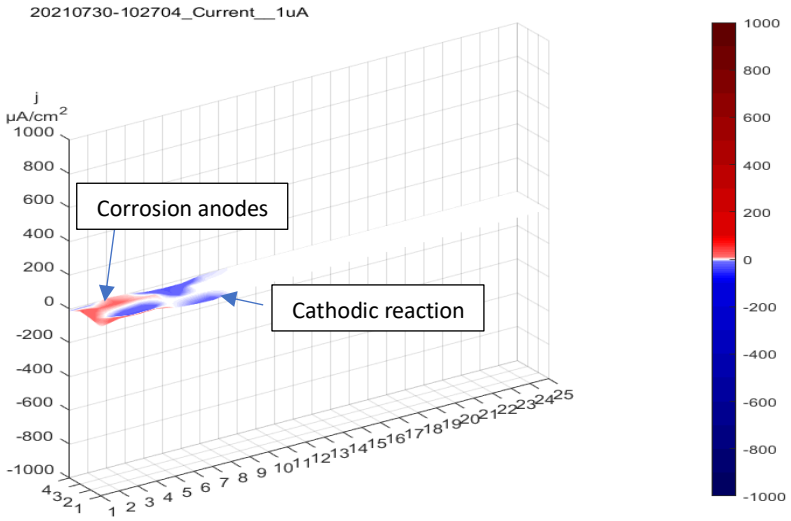

Figure 14(a): Addition of 0.01M/L $NaSO_4$ solution to sand

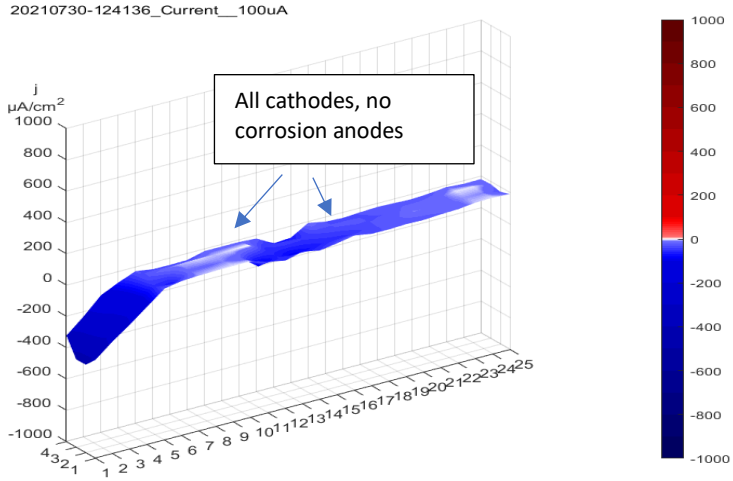

Figure 14(b): 0.01M/L $NaSO_4$ solution saturated sand with CP applied for 2 hours

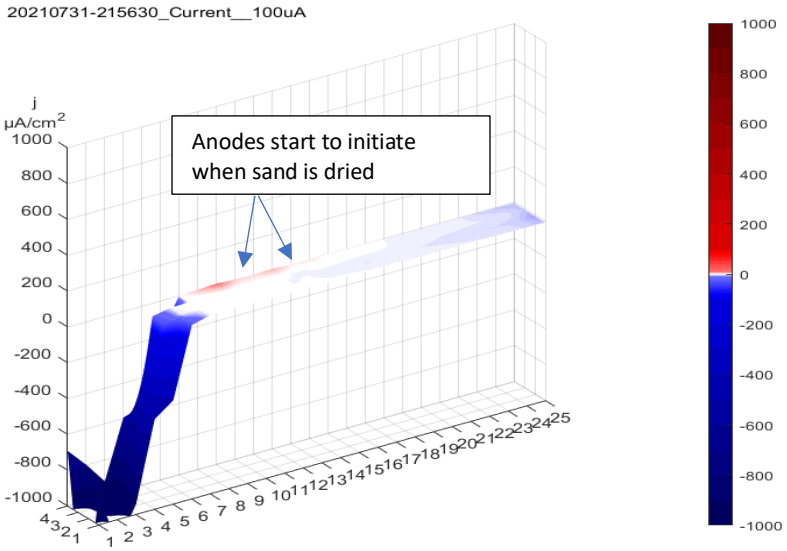

Figure 14(c). After 12 hours of draining the solution from the sand box

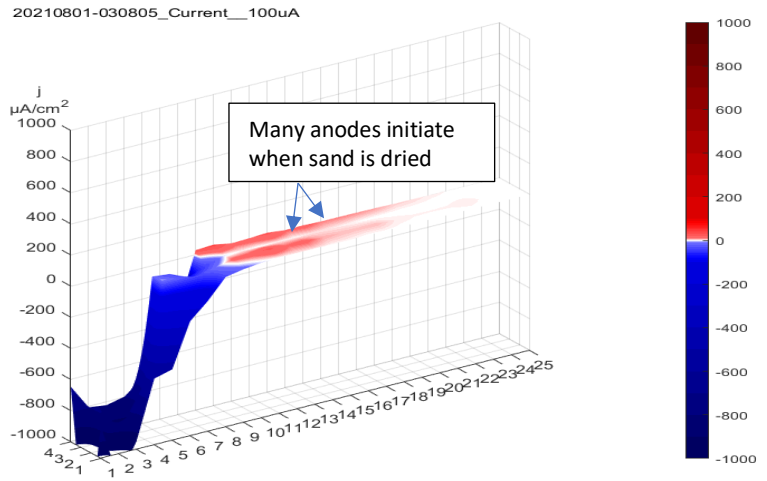

Figure 14(d): After 14 hours 57 minutes of draining the solution from the sand box.

Figure 14. A sample series of current density distribution maps recorded at various test periods from a sandbox testing cell that simulates a corrosion probe buried in a sandy soil environment under CP and wet-dry conditions

4. CONCLUSIONS

Field and sand box testing results repeatedly show that CUDC corrosion occurs when there is a wet-dry change in sand, simulating wet-dry seasonal changes. Many anodes appear under the crevice area simulating disbonded coating, suggesting the wet-dry cycle is a major factor in the initiation of CUDC. These results also illustrate CP potential as a critical factor affecting CUDC on buried pipeline exposed to unsaturated soil.

5. ACKNOWLEDGEMENTS

This work is funded by the Future Fuels CRC, supported through the Australian Governments' Cooperative Research Centres Program. The cash and in-kind support from the industry, government and university participants is gratefully acknowledged.

Industry Advisers, in particular Alan Creffield (APA, Lead Industry Adviser), Craig Bonar (APA), Phil Colvin (Jemena), Alan Bryson (CCE), Alireza Kouklan (AusNet), Bruce Ackland (Consultant), John Grapiglia (CCE), Myles Young (ROSEN), William Hughson (SEA Gas), Peter Wade (Energy Safe Victoria) for their advice and comments on our research proposal and on this work.

6. REFERENCES

1. *H. Leidheiser Jr, W. Wang Jr, L. Igetoft, The mechanism for the cathodic delamination of coatings from a metal surface, Progress in organic coatings, 11 (1983) 19–40.*
2. *M. Kendig, R. Addison, S. Jeanjaquet, The mechanism of cathodic disbanding of hydroxy-Terminated polybutadiene on steel from acoustic microscopy and surface energy analysis, J. Electrochem. Soc. 137 (1990) 2690–2697.*
3. *P.C. Rosa Rodrigues, C. Fernández, Influence of applied potential and temperature on the cathodic disbondment for offshore structures, Paper presented at the CORROSION 2011, Paper Number: NACE-11038, Houston, Texas, March 2011.*
4. *H. Bi, J. Sykes, Cathodic delamination of unpigmented and pigmented epoxy coatings from mild steel, Progress in organic coatings, 90 (2016) 114–125.*
5. *M. YJ. Tan. F. Varela, F. Mahdavi, M. Latino, K. Wang, A. Bryson, Bruce Ackland, Geoff Cope and M. Dragar, Recent progresses in understanding factors affecting cathodic disbondment and corrosion under disbonded coatings, the 22nd Biennial Joint Technical Meeting (JTM) to be held in Brisbane, Australia, 28 April to 3 May 2019*
6. *Fariba Mahdavi, Mike Yongjun Tan and Maria Forsyth, Communication—An Approach to Measuring Local Electrochemical Impedance for Monitoring Cathodic Disbondment of Coatings, Journal of The Electrochemical Society, 163 (5) C228-C231 (2016)*
7. *F. Mahdavi, M.Y.J. Tan and M. Forsyth, Electrochemical impedance spectroscopy as a tool to measure cathodic disbondment on coated steel surfaces: Capabilities and limitations, Prog. Org. Coat. 88, 23 (2015)*
8. *Mahdavi F, Forsyth M, Tan MYJ, Understanding the effects of applied cathodic protection potential and environmental conditions on the rate of cathodic disbondment of coatings by means of local electrochemical measurements on a multi-electrode array, Progress in organic coatings 103:83-92 (10 pages) 2017*
9. *M. Latino, Measuring and understanding cathodic protection current through disbonded organic coatings and its effect on corrosion, PhD thesis, Deakin University (2018)*
10. *M. Latino, F. Varela, M. Forsyth, Y. Tan, Self-validating electrochemical methodology for quantifying ionic currents through pipeline coatings, Progress in Organic Coatings, 120 (2018) 153-159*
11. *F. Varela, M. Y.J. Tan and M. Forsyth, Electrochemical method for studying localised corrosion beneath disbonded coatings under cathodic protection, Journal of the Electrochemical Society 162(10):C515-C527 (2015)*
12. *F. Varela, M. Y.J. Tan and M. Forsyth, An electrochemical method for measuring localised corrosion under cathodic protection. ECS Electrochemistry Letters 4(1):C1-C4 (2015)*
13. *F. Varela, M.Y.J. Tan, M. Forsyth, Understanding the effectiveness of cathodic protection under disbonded coatings, Electrochimica Acta, 186:377-390 (2015)*
14. *K. Wang, F. B. Varela and M. YJ Tan, "Probing dynamic and localised corrosion processs on buried steel under coating disbondment of various geometries", Corrosion Science, in press (accepted 21/01/2019), https://doi.org/10.1016/j.corsci.2019.01.034*
15. *K. Wang, F. B. Varela and M. YJ Tan, "Visualizing dynamic and localized corrosion on cathodically protected steel buried in soil with different moisture contents", Corrosion (NACE), in press (accepted 01/01/2019), https://doi.org/10.5006/3080*
16. *Y. Tan, Y. Huo, F. Varela, K Wang, A New Approach to Probing Localized Corrosion of Pipelines, Materials performance 60(2):5 pages 2021*
17. *Y Tan Y, F Varela, Y Huo, Field and laboratory assessment of electrochemical probes for visualizing localized corrosion under buried pipeline conditions, Journal of Pipeline Science and Engineering 1(1):88-99 Mar 2021*